Journal of Applied Polymer Science

Palm Oil-Based Organogels and Microemulsions for Delivery of Antimicrobial Drugs

Suryakant Pradhan,[1] Satish S. Sagiri,[1] Vinay K. Singh,[1] Kunal Pal,[1] Sirsendu S. Ray,[1] Dillip K. Pradhan[2]

[1]Department of Biotechnology and Medical Engineering, National Institute of Technology, Rourkela 769008, Odisha, India
[2]Department of Physics, National Institute of Technology, Rourkela 769008, India
Correspondence to: K. Pal (E-mail: pal.kunal@yahoo.com)

ABSTRACT: This study has been designed to develop palm oil (PO) based organogels using span 80/tween 80 mixture (OG) as a gelator system by fluid-filled structure mechanism. The results suggested formation of organogels, emulsions, and microemulsions as the proportions of PO, OG and water were varied. The emulsions were found to be thermodynamically unstable as compared to the organogels and the microemulsions. Accelerated thermal stability test suggested that all the microemulsions and the organogels of only eight compositions were stable. The organogels showed viscoelastic property while the microemulsions showed viscous flow behavior. Both the organogels and the microemulsions were found to be highly hemocompatible and nonirritant. The antimicrobial efficiency of the ciprofloxacin HCl-loaded formulations showed equivalent efficiency as compared to marketed formulations. The rates of drug release from the organogels were found to be relatively slower as compared to the microemulsions. The preliminary studies suggested that the developed organogel and microemulsion-based formulations may be tried for topical delivery of antimicrobials. © 2013 Wiley Periodicals, Inc. J. Appl. Polym. Sci. **2014**, *131*, 39979.

KEYWORDS: biocompatibility; drug delivery systems; gels; microscopy

Received 27 June 2013; accepted 17 September 2013
DOI: 10.1002/app.39979

INTRODUCTION

In recent past, topical drug delivery systems have gained much importance due to the ease in the application of formulations (e.g., ointments, gels and lotions).[1] Of late, there has been an exponential increase in the use of gel-based delivery vehicles. This may be attributed to the ease of formulation of the gel-based delivery vehicles with desirable properties.[2] A gel-based delivery system may be classified either as hydrogel or as organogel. Hydrogel immobilizes polar solvents while organogel immobilizes apolar solvents.[3–6] Immobilization of the solvents takes place due to the formation of meshed structure by a solid component generally regarded as gelator. Because of the ease of preparation and inherent thermodynamic stability of the organogels, organogels have evolved as a topic of research interest amongst the pharmacists and food scientists.[7] The gelator molecules responsible for the development of organogels are regarded as organogelators. The mechanism of gellation may be achieved by forming 3D networked structures either by solid fiber or by fluid-filled fiber/structures. Various ionic (e.g., sodium lauryl sulphate, sodium stearate, etc.) and nonionic (e.g., polysorbates, sorbitan esters, poloxamer, etc.) surfactants have been used as gelator molecules for the development of organogels.[8] Unlike ionic surfactants, nonionic surfactants are nonirritant. This property of the nonionic surfactants has facilitated the exploitation of nonionic surfactants for the development of organogels. A broad category of sorbitan esters-based nonionic surfactants have gained wide applications in pharmaceutical and food industries.[9–11] The solid surfactants help in formation of organogels by solid fiber mechanism while liquid surfactants forms organogels by forming fluid-filled structures. In either of the case, there are physical interactions amongst the solid fiber or fluid-filled structures to form networked structures.[12] The physical forces responsible for the formation of the 3D networked structure include van der waals interactions,[13] π-π interactions,[14] and hydrogen bonds.[15] Gelation of vegetable oils by nonionic surfactants provides vast opportunities for the delivery of bioactive agents.[16] This may be associated with the versatility and biocompatibility of these organogels.[17]

Microemulsions may be defined as biphasic isotropic systems consisting of a surfactant, oil, and water. Depending on the composition of the formulation, a microemulsion may or may not contain a cosurfactant. They are transparent in nature and have been found to be thermodynamically stable. In recent

Table I. Instrumental Parameters for Texture Analysis

		Testing conditions			
Type of study	Type of fixture	Pre test speed (mm/s)	Test speed (mm/s)	Post test speed (mm/s)	Mode of study
Gel strength	P/3 3mm diameter cylindrical probe	1.0	1.0	10.0	Button mode (5 mm)
Stress relaxation	HDP/SR spreadability rig with 45° conical perspex probe	1.0	0.5	10.0	Auto force (5g; 5 mm)
Spreadability	HDP/SR spreadability rig with 45° conical perspex probe	2.0	2.0	2.0	Button mode (23 mm)
Backward extrusion	A/BE back extrusion rig	1.0	1.0	1.0	Button mode (20 mm)

years, microemulsion-based formulations have gained much attention to be used as vehicle for controlled delivery. Sorbitan ester (e.g., span 80 and tween 80) based microemulsions have been studied in-depth. Microemulsion-based organogels have been tested successfully in cutaneous drug delivery to improve the bioavailability.

Palm oil (PO) is edible oil and is commonly used in South-East Asia.[18] It is extracted from the fruits of palm tree (Elaesis guineenis). It has attracted much attention as a raw material for the development of drug delivery systems due to its beneficial properties (e.g., thermal and chemical stability). Because of its beneficial properties, PO has been extensively studied in food industries. PO-based derivatives have been studied for the formulation of emulsions including micro/nanoemulsions.[19]

Taking inspiration from the above, attempts were made to prepare span 80-tween 80-based formulations using palm oil (PO) as the vegetable oil. The developed PO-based formulations were characterized thoroughly to be used for controlled delivery of antimicrobial agents.

MATERIALS AND METHODS

Materials

Sorbitan monooleate (SM; Span80), and polyoxyethylene sorbitan monooleate (PM; Tween 80) were obtained from Lobachemie, Mumbai, India. Dialysis membrane (molecular weight cut off: 12–13 kDa) was procured from Himedia, Mumbai, India. Palm oil (PO) was purchased from the local market. Ciprofloxacin HCl (CFX) was received as a gift from Lupin Pharmaceuticals, Pune, India. Fresh goat blood was obtained from the local butcher shop. Double distilled water (DW) was used throughout the study.

Preparation of Organogels

SM and PM were mixed in the ratio of 1:2 (w/w) to form a homogeneous mixture. This mixture was used as an organogelator (OG). The preparation of organogels was carried out by fluid-filled fiber mechanism as per the reported literature.[20] Organogels were prepared by mixing specified amount of OG in PO at room temperature (RT; 25°C). The mixture was homogenized at 200 rpm for 10 min. To this mixture of OG and PO, DW was added drop-wise with constant vortexing. Depending on the composition of the mixture, the mixture either formed organogels or remained as liquid. The liquid formulations were either transparent (microemulsion) or opaque (emulsion). Mapping of the compositions of the formulations was done using a ternary phase diagram plot. Preliminary studies suggested quick destabilization of emulsion; hence emulsions were not further studied. Drug-loaded organogels and microemulsions were prepared by dissolving required amount of CFX in DW and using the aqueous solution of the drug for the preparation of the formulations. The amount of the drug dissolved in DW was such that the final concentration of the drug in the formulation was 1% (w/w). The rest of the procedure for sample preparation was same.

Accelerated Thermal Stability Studies

Thermocycling method of accelerated stability test was used to analyze the long-term stability of the organogels and microemulsions as per the previously reported method.[21,22] In short, the samples were incubated alternatively at 80°C for 15 min in a water bath (Remi, Mumbai, India) and subsequently at −20°C temperature controlled cabinet for the next 15 min. This constituted 1 cycle. The experiment was continued for 5 cycles. The samples were continuously monitored for any signs of destabilization. The microemulsions and the organogels were regarded as destabilized if there was a phase separation. Organogels were also regarded as destabilized if they failed to maintain their structural integrity. The samples were regarded as stable, if they were able to sustain 5 cycles of thermocycling without any signs of destabilization.

Organoleptic Evaluation

Freshly prepared organogels and microemulsions were observed for their color, odor, appearance, and texture.[23]

Microscopic Studies

The microstructure of the organogels were analyzed under bright field microscope (BFM) (LEICA-DM 750 equipped with ICC 50-HD camera, Germany). The organogels were converted into xerogels and subsequently visualized under scanning

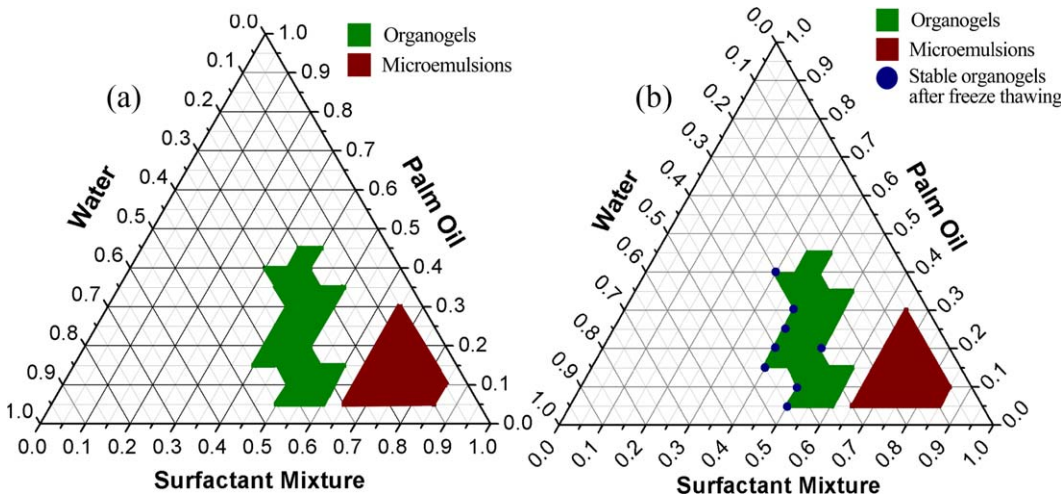

Figure 1. Pseudo-ternary phase diagram (Triplot) of freshly prepared formulations and stable formulations after freeze-thaw test. [Color figure can be viewed in the online issue, which is available at wileyonlinelibrary.com.]

electron microscope (SEM) (JEOL, JSM-6390, Japan). The xerogels were then sputter coated with platinum prior to the SEM analysis. The microstructures of the microemulsions were visualized under phase contrast microscope ((PCM; Carl Zeiss, Model HBO 50, Germany).

Fourier Transform Infrared Spectroscopy

The interactions amongst the components of organogels and microemulsions were analyzed by Fourier Transform Infrared (FTIR) spectroscopy using alpha-E, Bruker, Germany. The analysis was conducted in attenuated total reflectance (ATR) mode.

X-ray Diffraction (XRD) Analysis

The organogels were analyzed by X-ray diffractometer (Panana-lytical X'PERT MPD XRD Machine, Netherlands) using Cu-Kα radiation, generated at 30 KV and 20 mA. The scanning range was 5° to 50° 2θ at a step size of 2°/min. The analysis was performed at RT. The XRD of the microemulsions were not studied due to the instrumental limitation to handle liquid sample.

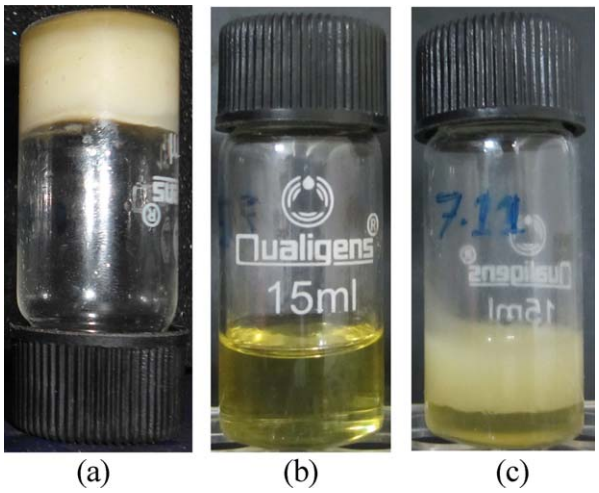

Figure 2. Representative samples. (a) Organogel, (b) Microemulsion, and (c) Phase separated systems. [Color figure can be viewed in the online issue, which is available at wileyonlinelibrary.com.]

Thermal Analysis

The gel to sol transition (T_{gs}) of the organogels was determined by falling ball method as per the previously reported literature.[24] In short, 2 g of the organogels was poured in a 10 mL test tube. A stainless steel (SS) ball (diameter: 1/8th of an inch; weight= 130 mg) was placed gently on the top of the organogels. The test tube was heated at a rate of 1°C/min in a melting point determination apparatus (EI melting point apparatus 931). The temperature at which the SS ball started to move into the gel was noted as the T_{gs} of the organogels.

Thermal properties of the representative organogels and the microemulsions were investigated using differential scanning calorimeter (DSC; DSC-200 F3, MAIA, Netzsch, Germany) over a temperature range of 20°C to 150°C at a heating rate of 2°C/min under N_2 environment. Aluminum (Al) crucibles with pierced Al lid were used as the sample holder for the study.[25]

Texture Analysis

The textural properties of the organogels and the microemulsions were studied using a texture analyzer (Stable Microsystems, TA-HDplus, UK). Backward extrusion (BE), gel strength, spreadability, and stress relaxation studies were performed at RT. The instrumental parameters for the textural analysis have been given in Table I. The apparent dynamic viscosity of the samples was predicted using BE study. DW was taken as the reference sample for viscometric analysis using texture analyzer. The apparent dynamic viscosity of DW at 37°C was taken as 0.693 mPa s. The apparent dynamic viscosity of the samples was calculated using the following equations[26]:

$$\eta_{app} = K \times \frac{df}{dx} \quad (1)$$

$$K = \frac{R_c^2 - R_p^2}{2\ \pi\ R_c^2 C_1 \nu_p} \quad (2)$$

$$\eta_{Sample} = \eta_{Water} \frac{(df/dx)_{Sample}}{(df/dx)_{Water}} \quad (3)$$

where η_{app} is the apparent dynamic viscosity, K is a constant; df/dx is the slope of the force vs. distance curve of BE profile

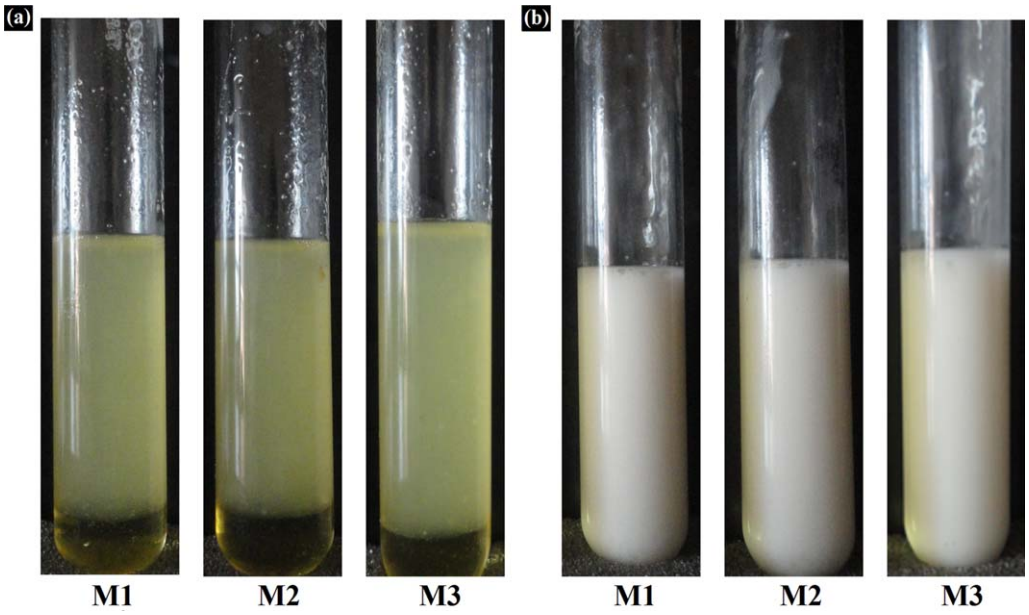

Figure 3. Dilution test of microemulsions. (a) Phase separation in PO, and (b) Homogenous mixture in DW. [Color figure can be viewed in the online issue, which is available at wileyonlinelibrary.com.]

when the probe is retracting. The R_c and R_p are the cup and probe radii, υ_p is the probe velocity and C_1 is the instrument constant.

Electrochemical Impedance Spectroscopy

The electrical properties of the developed organogels were studied using a computer-controlled impedance analyzer (Phase sensitive multimeter, Model: PSM1735, Numetriq, UK). The impedance spectroscopic measurement was done by applying an AC voltage of 100 mV across the SS plate /gel/SS plate sample holder as a function of frequency 0.1 Hz–10 MHz at RT.[27] The electrical impedances of the microemulsions were outside the measurement limits of the instrument.

In Vitro Drug Delivery Studies

The *in vitro* drug release studies were carried out using a modified Franz's diffusion cell.[21,28] Dialysis membrane was used to separate the donor and the receptor chambers. Accurately weighed samples (~2 g) were loaded in the donor compartment and placed gently in to the receptor compartment so that the dialysis membrane was in contact with the receptor fluid. Totally, 50 mL of DW was used as the dissolution medium and was kept on stirring at 100 rpm and the temperature was maintained at 37 ± 1°C. The receptor fluid was replaced at regular intervals of time (15 min during first hour and subsequently for every 30 min in the next 7 h). The samples were then analyzed using UV-visible spectrophotometer at 271 nm (UV-3200, LABINDIA, Mumbai, India).

Table II. Stable Organogels After Freeze-Thaw Test

Samples	OG (g)	Oil (g)	Water (g)	W/OG ratio
A	50.0	5.0	45.0	0.9
B	50.0	10.0	40.0	0.8
C	40.0	15.0	45.0	1.125
D	40.0	20.0	40.0	1.0
E	50.0	20.0	30.0	0.6
F	40.0	25.0	35.0	0.875
G	40.0	30.0	30.0	0.75
H	30.0	40.0	30.0	1.0

Antimicrobial Studies

The antimicrobial activity of the drug loaded organogels and microemulsions were tested against *Bacillus subtilis* (MTCC 121). Totally, 50 µL of bacterial suspension (10^5 to 10^6 CFU/mL) was spread over the petri-plates containing nutrient agar medium. Bores of 9 mm diameter was made using a SS borer. Ciplox® gel was used as the positive control. The organogels or microemulsions without drugs were used as the negative control. The

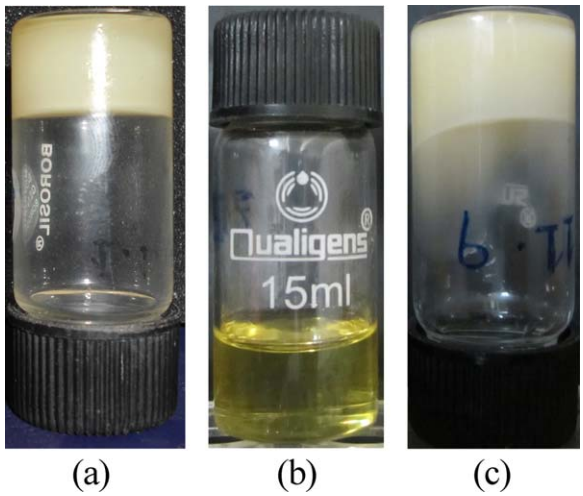

Figure 4. Representative samples after accelerated thermal stability test. (a) stable organogel, (b) stable microemulsion and (c) unstable organogel. [Color figure can be viewed in the online issue, which is available at wileyonlinelibrary.com.]

Table III. Composition of the Representative Organogels and Microemulsions Used for Further Analysis

Sample code	OG (% w/w)	Palm oil (% w/w)	DDW (% w/w)	CFX (% w/w)
G1	40.0	20.0	40.0	–
G2	50.0	20.0	30.0	–
G3	40.0	30.0	30.0	–
M1	70.0	20.0	10.0	–
M2	70.0	10.0	20.0	–
M3	80.0	10.0	10.0	–
G1D	40.0	20.0	39.0	1.0
G2D	49.0	20.0	30.0	1.0
G3D	39.0	30.0	30.0	1.0
M1D	69.0	20.0	10.0	1.0
M2D	69.0	10.0	20.0	1.0
M3D	79.0	10.0	10.0	1.0

inoculated plates were then incubated at 37 ± 1°C for 24 h to allow bacterial growth. The effect of the drug on bacteria was observed by measuring the zone of inhibition using a ruler.

RESULTS AND DISCUSSION

Preparation of Organogels and Microemulsions

The organogels and the microemulsions were prepared by mixing OG and PO, followed by drop-wise addition of DW with constant vortexing. The formation of organogel was confirmed by inverted test-tube method.[23] The samples which did not show any flow have been regarded as organogels [Figure 2(a)]. In addition to the organogels, emulsions, and microemulsions were also formed at some compositions [Figure 1(a)]. But the emulsions were found to be thermodynamically unstable and showed phase separation [Figure 2(b)] and hence were not considered for further studies. Microemulsions are transparent emulsions [Figure 2(c)] often having the dispersed phase diameter in the sub-micron range.[29,30] The mapping of the formulations suggested that the organogels were formed when the concentration of the OG, PO, and DW were in the ranges of 30–60%, 5–45%, and 15–45%, respectively (Figure 1). At these proportions, the OG was able to form DW-filled spherical or fiber-like aqueous structures. These fluid-filled structures interacted with each other to form a 3D network, which in turn, resulted in the immobilization of the PO.[20] On the other hand, microemulsions were formed when the concentration of the OG, PO, and DW were in the ranges of 65–85%, 5–30%, and 5–30%, respectively (Figure 1). This suggested that at higher concentrations of surfactant mixture, microemulsions were formed. Formation of microemulsions at higher concentration of surfactants is quite common in edible oil/water compositions.[29] It has been previously reported that the formation of non-ionic microemulsions is possible upon dilution of edible oil-surfactant mixture with water.[31] Because of this phenomenon, the dilution of PO-OG mixture with DW resulted in the formation of microemulsions. As per the Winsor classification, if the surfactant is soluble in aqueous phase then the

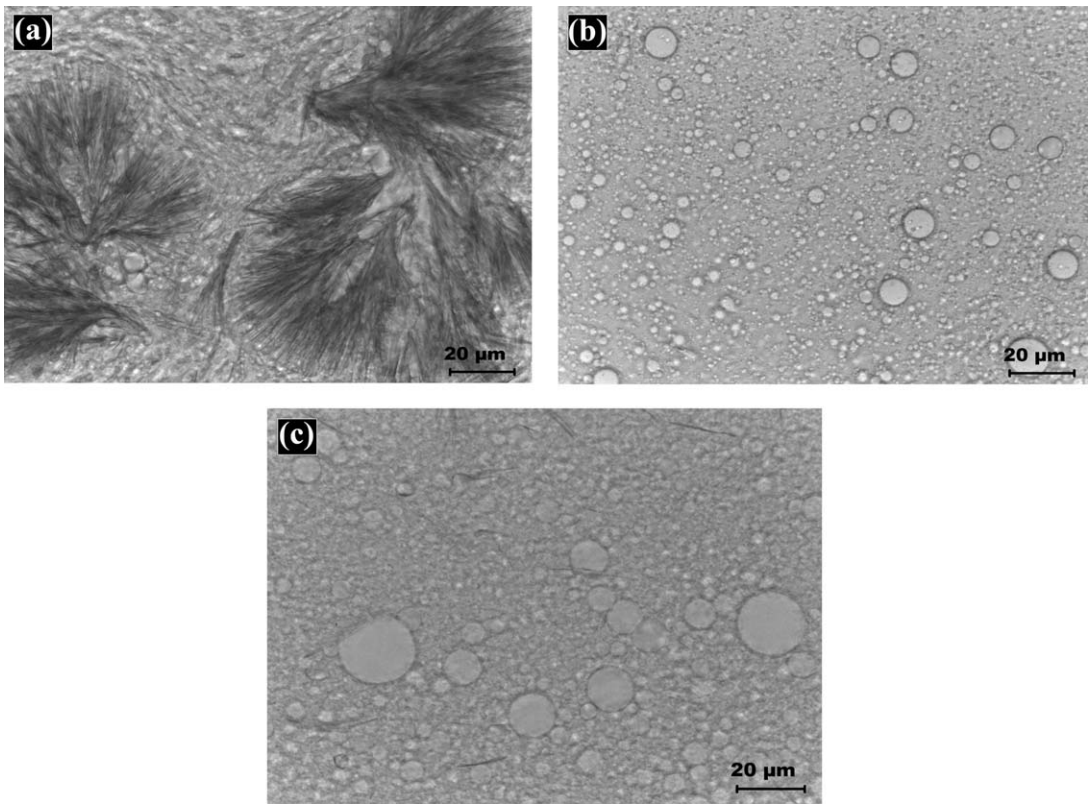

Figure 5. BFM micrographs at 40× magnification. (a) G1, (b) G2, and (c) G3.

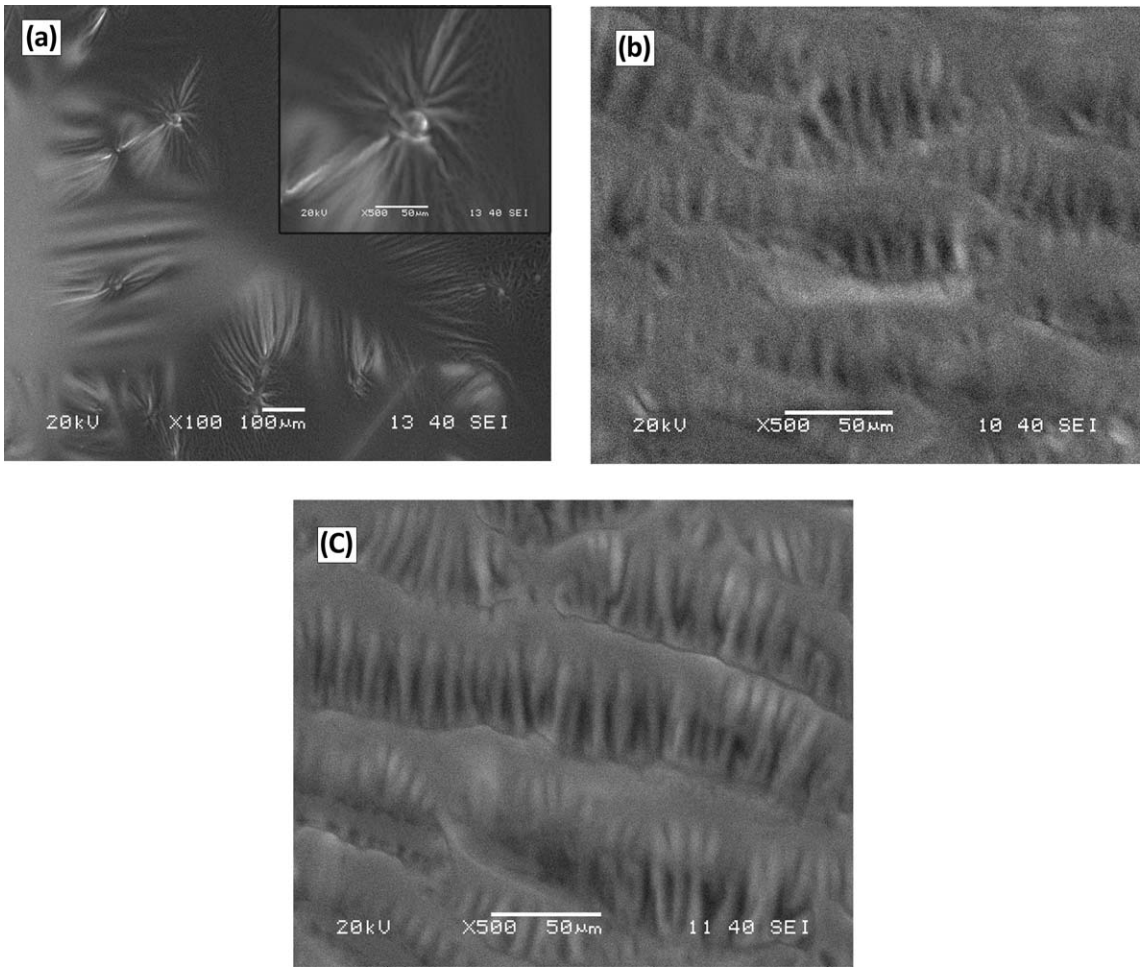

Figure 6. SEM micrographs at 100× magnification. (a) G1, (b) G2, and (c) G3.

microemulsions are regarded as the Winsor Type-I microemulsion.[32] In this study, a mixture of span 80: tween 80 (1:2) was used. The HLB value of the surfactant mixture was found to be ~11. This suggested that the surfactant mixture might result formation of oil-in-water microemulsions. The type of the microemulsion was determined by dilution test. One gram of the microemulsion was added to 4 g of either PO or DW and mixed thoroughly. The results showed a phase separation when the microemulsions were added to PO while they formed a homogenous white mixture in DW (Figure 3). The results confirmed that the microemulsions formed were oil-in-water microemulsions.

Even though the reorganization of the surfactant molecules is responsible for the formation of the organogels, a higher proportion of OG did not form organogels but a microemulsion. This may be explained by the fact that in microemulsions there was a lower proportion of DW. The amount of DW was not sufficient to induce self-assembly of the OG. Since the amount and the size of dispersed particles was considerably low in microemulsion, the interfacial tension at the interface of the oil and water was very low.[33] This resulted in the improved thermodynamic stability of the microemulsions. To stabilize the small-sized dispersed droplets, there is a need for higher proportions of surfactants molecules.[34] In organogels, the proportion of DW was above the critical limit to induce gelation.[35]

The pH of the developed formulations was within the limits of the skin pH and it is expected that the formulations may be used in controlled delivery applications.[20] % hemolysis of organogels and microemulsions was found to be less than 5, which can be considered as highly hemocompatible.[23] Hence, the developed organogels and microemulsions may be regarded as biocompatible and may be used for biological applications.

Accelerated Thermal Stability Test

The stability of the organogels and the microemulsions were checked by accelerated thermal stability test. After five cycles of freeze-thaw, only eight organogels were found to be stable. All the microemulsions were stable after five cycles of freeze-thaw. The mapping of the stable organogels and microemulsions has been shown in [Figure 1(b), Table II]. One representative stable organogels and microemulsions samples along with a representative destabilized organogels have been shown in Figure 4. The results suggested that the stability of the organogels was affected by the DW to OG (W/OG) ratio. W/OG ratio in the stable organogels was within 0.6 and 1.125. On the other hand, the W/OG ratios of the unstable organogels were < 0.5. Higher

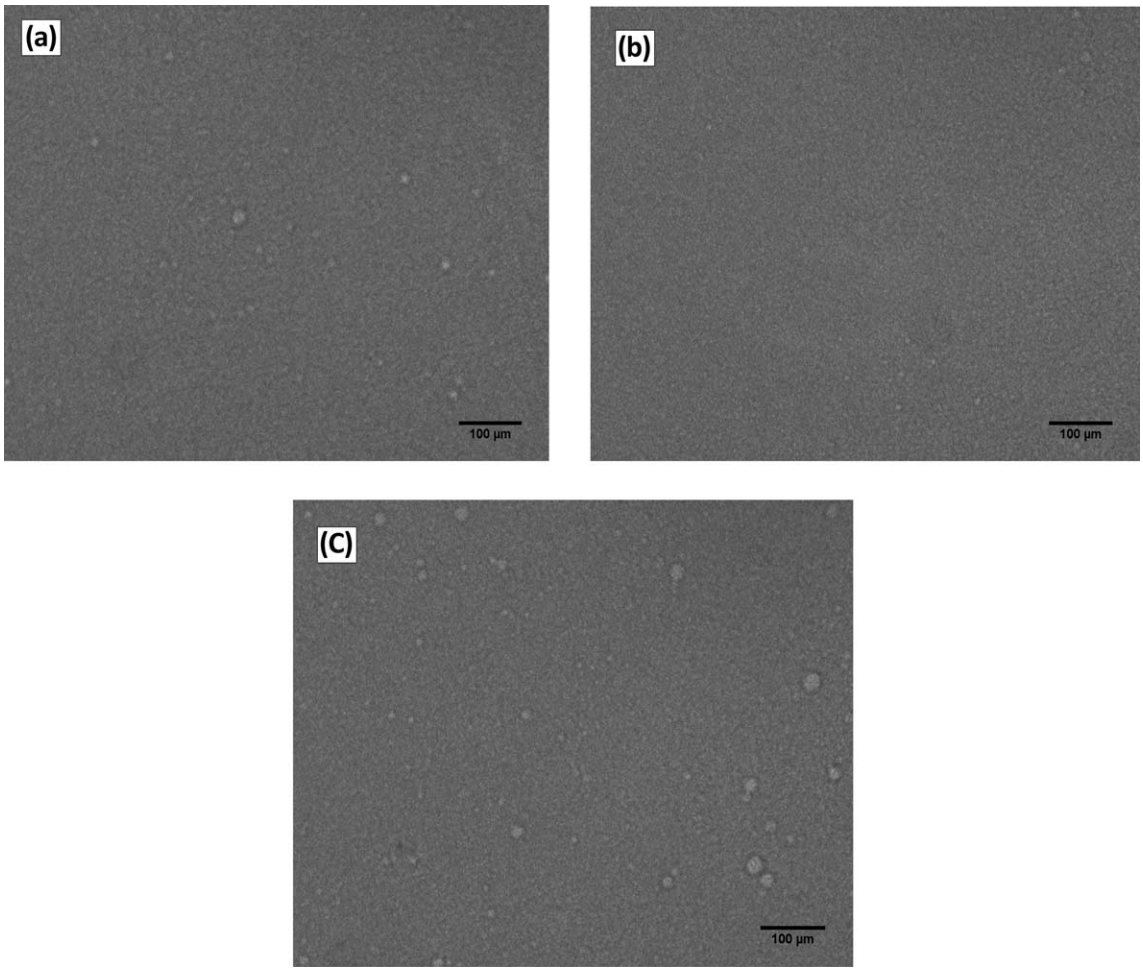

Figure 7. PCM micrographs at 20× magnification. (a) M1, (b) M2, and (c) M3.

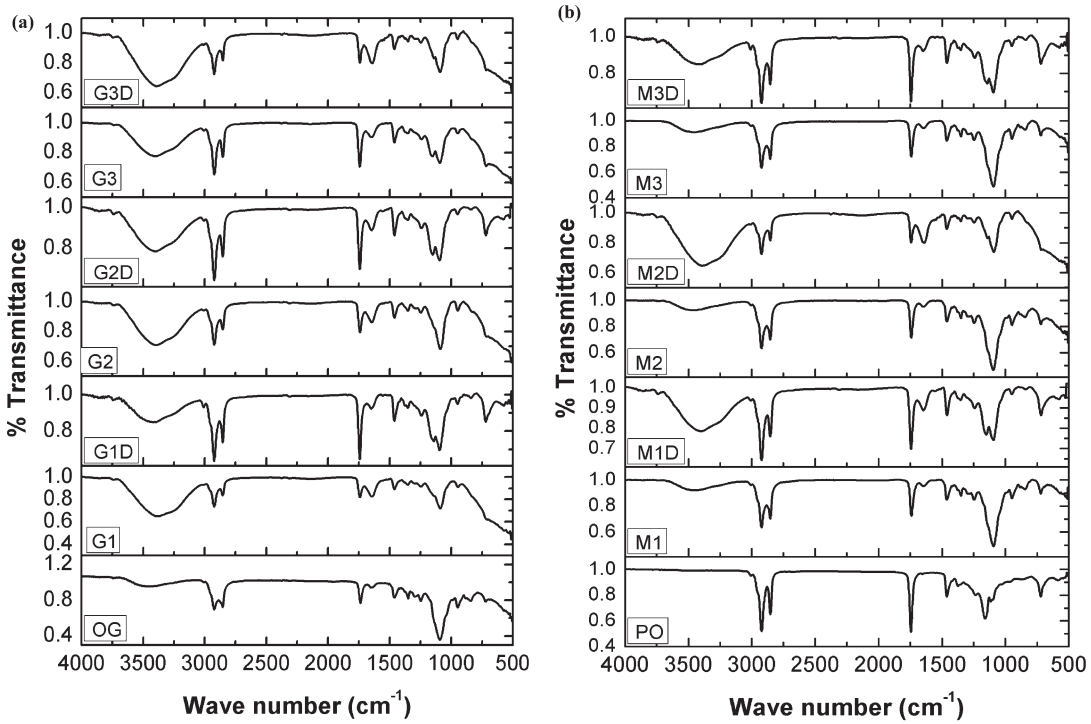

Figure 8. FTIR spectra. (a) OG and organogels, and (b) PO and microemulsions.

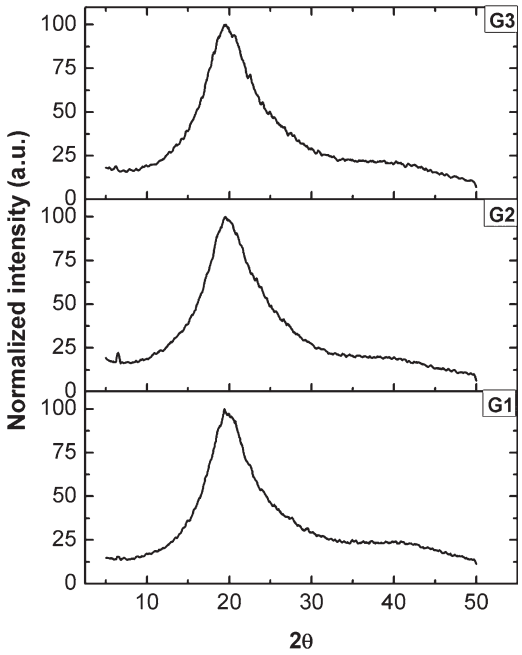

Figure 9. X-ray diffractograms of the organogels.

W/OG value might have lead to the formation of stronger molecular interactions amongst DW and OG, which in turn, might have improved the stability of the organogels.[36] 3 numbers of organogels and 3 numbers of microemulsions were chosen for further evaluation (Table III).

Organoleptic Evaluation

The color of the organogels varied from white to yellowish white and was dependent on the composition of the formulation. The increase in concentration of DW resulted in the increase in the whiteness of the organogels. All gels were opaque. They were oily to touch but the degree of oiliness was dependent on the proportion of DW in the organogels. Microemulsions were yellow in color and completely transparent. They were oily to touch. Both organogels and microemulsions had a bland taste.

Microscopic Studies

BFM micrographs of the representative organogels have been shown in Figure 5. Microstructure of the organogels was also affected by the W/OG ratio. Clusters of fluid-filled fibers were observed when the W/OG ratio was on the higher side. As the W/OG ratio was lowered, the occurrences of the fluid-filled fibers were reduced in G3 organogels and were not seen at all in G2 organogels. Presence of water lead to the formation of inverse micellar structures.[12] These structures self-assembled to form 3D fibrous network.[37] The self-assembly and aggregation of micelles was based on the molecular interactions (e.g., hydrogen bonding and π-π interactions).[38] PO was immobilized within this 3D networked structure to form organogel.

Table IV. The XRD Parameters of the Organogels

Sample	Peak position (2θ)	FWHM
G1	19.46	7.28
G2	19.36	8.24
G3	19.6	7.62

Table V. Gel-to-Sol Transition Temperature (T_gs) Determined by Falling Ball Method

Samples	T_{gs} (°C)
G1	44 ± 0.5
G2	41 ± 1.0
G3	40 ± 1.0

The architecture of the organogels was also analyzed by SEM studies by converting them into xerogels (Figure 6). The micrograph of G1 xerogel showed presence of clusters of gelator fibers. These clusters formed spherulitic networks [magnified spherulite has been shown as an insert in Figure 6(a)]. In organogels, spherulites can be formed by either homogeneous or heterogeneous nucleation mechanisms.[39] Under homogeneous nucleation mechanism, the gelator fibers/needles first form in the solution and subsequently split at the tip and the branches evolve to a sheaf-like morphology. In case of heterogeneous nucleation mechanism, fibers grow radially outward from a spherical center. The insert of Figure 6(a) shows the radial outgrowth of gelator fibers from the center, signifying the possibility of formation of spherulites by heterogeneous nucleation. SEM micrographs of G2 and G3 showed the presence of layered structures of inverse micelles. The density of the micelles was more in G3 than G2. This may be attributed to the presence of higher W/OG ratio in G3. The presence of inverse micellar structures in G2 were not visible in BFM but were visualized under SEM. This might be due to the low magnification in BFM because of which the fibrous structures were not observed.

The PCM micrographs of the microemulsions have shown the presence of spherical dispersed phase (Figure 7). The average particle size of the dispersed phase of M1, M2, and M3 was 4.9 ± 2.31 μm, 4.17 ± 2.21 μm, and 10.56 ± 2.88 μm, respectively. The increase in the concentration of DW in M2 resulted in the decrease in the average particle size of the dispersed phase. On the other hand, an increase in the OG in M3 resulted in the increase in the size of the globular particles. Also, there was aggregation of the particles in M3. Increase in the oil fraction in M1, resulted in the formation of globular particles having sizes in between M2 and M3.

FTIR Studies

The chemical interactions amongst the organogel and microemulsion components were studied by ATR-FTIR (Figure 8). The FTIR spectra of OG and organogels were found to be similar except the intensity of the peak at 3500 cm^{-1}. The increase in the intensity of the peak of organogels may be attributed to the formation of intermolecular hydrogen bonding between the carboxyl groups of fatty acids and –OH groups of DW.[40] This indicated that intermolecular hydrogen bonding played an important role in the formation of the organogels. The increase in the peak intensity at 3500 cm^{-1} was also found in the microemulsions. Intermolecular hydrogen bonding might also have been present in the microemulsions as well. The incorporation

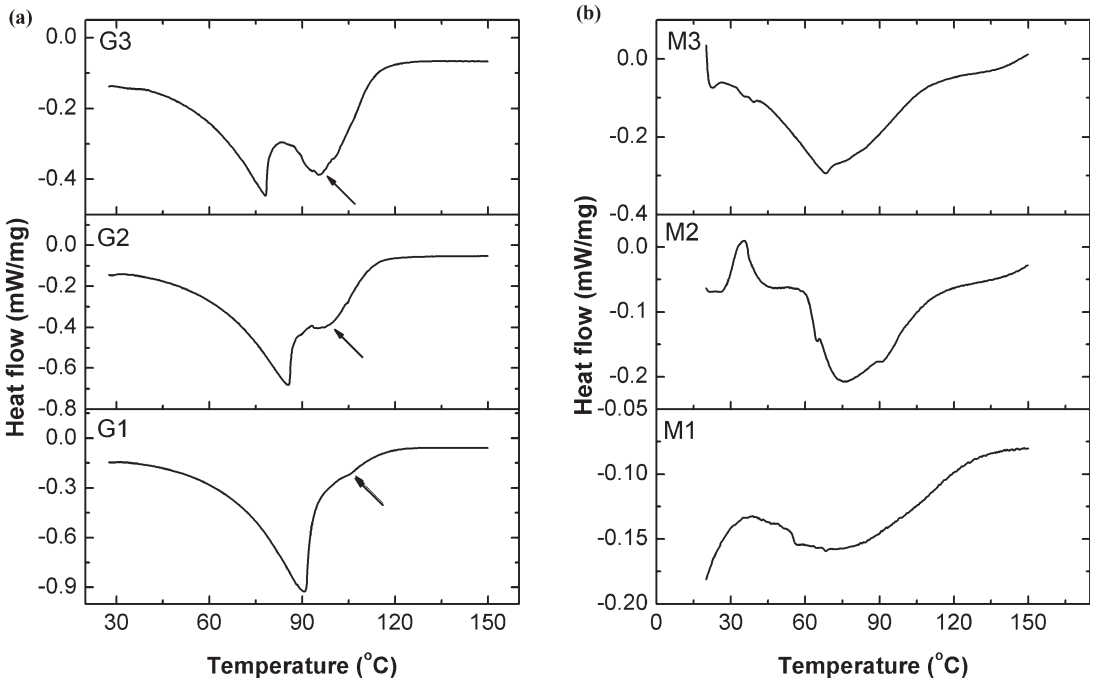

Figure 10. Thermal profiles of the formulation studied using DSC. (a) Organogels and (b) Microemulsions.

of CFX did not cause any change in the FTIR spectra of the organogels and microemulsions. This may be due to the presence of drug in minute concentrations and the peaks of the drugs were subsided because of the peaks of the organogel and microemulsion components which were present in much higher proportions.

XRD Analysis

XRD profiles of the organogels have been shown in Figure 9. The organogels were found to have a single broad peak at ~20° 2θ. The presence of broad peak suggested the amorphous nature of the organogels. The XRD parameters of the organogels have been tabulated in Table IV. The change in crystallinity of the

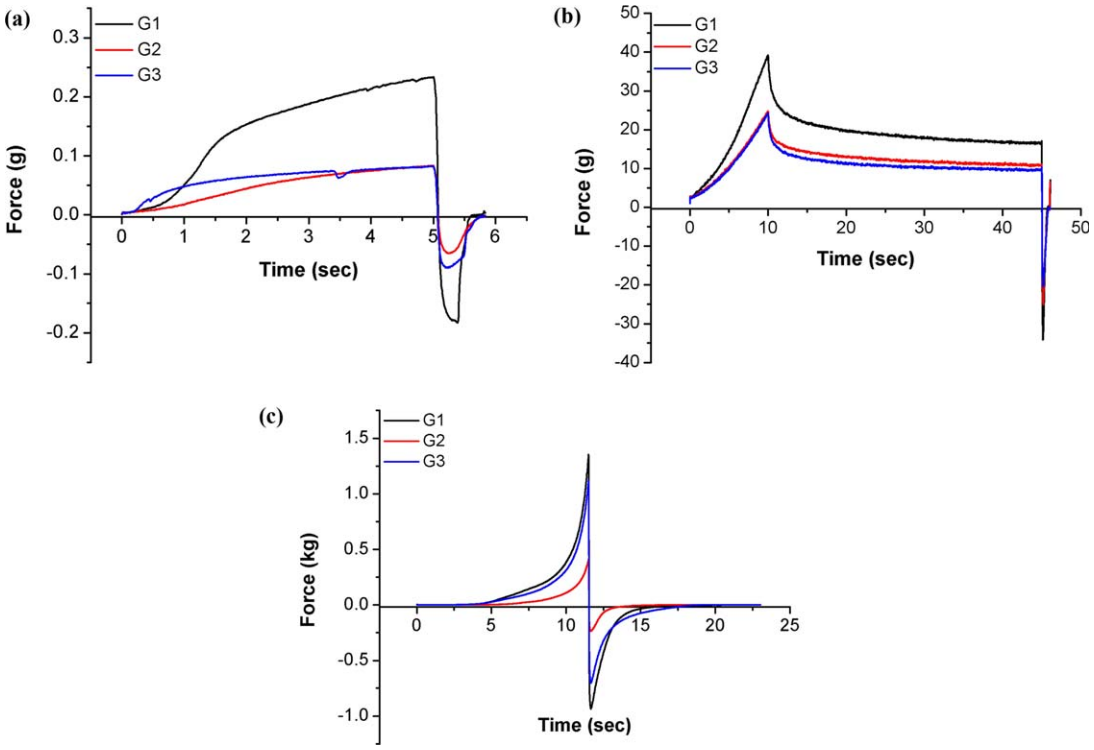

Figure 11. Textural properties of the organogels. (a) Gel strength, (b) stress relaxation, and (c) spreadability. [Color figure can be viewed in the online issue, which is available at wileyonlinelibrary.com.]

Table VI. Textural Properties of the Organogels (Gel Strength Parameters)

Samples	Hardness (g)	Rigidity (g s)	Stickiness (g)	Adhesiveness (g)
G1	119.02	59.039	−182.851	−60.324
G2	31.24	21.060	−65.551	−26.526
G3	57.15	53.638	−89.966	−38.987

organogels was estimated by calculating the full width at half maximum (FWHM) from the diffractograms. The FWHM of the organogels was in the order of G1<G3<G2. The results suggested that the crystallinity of the G1 was highest followed by G3 and G2. This observation may be associated with the presence of higher W/OG ratio in G1 followed by G3 and G2. The presence of higher W/OG ratio improved the intermolecular hydrogen bonding (as was also evident from FTIR studies), which in turn, resulted in improved crystallinity in organogels.[21]

The XRD of the microemulsions were not conducted due to the limitation of the instrument to handle liquid samples.

Thermal Analysis

The gel-to-sol transitions (T_{gs}), as determined by the falling ball method, of the organogels have been tabulated in Table V. Higher T_{gs} values were obtained for the G1 gels followed by G2 and G3. The difference in the T_{gs} of the G2 and G3 was not significant. The differences in the T_{gs} values may be associated with the intermolecular hydrogen bonding/crystallinity of the organogels. This, in turn, may be related to the W/OG ratio in the organogel samples. Since the microemulsions were liquid at RT, the T_{gs} study was not possible.

The thermal profiles of the organogels and the microemulsions were studied by DSC (Figure 10). The organogels have shown a broad endothermic peak at ~90°C which may be associated with the evaporation of free water in the organogels. The intensity of the peak was highest in G1 followed by G2 and G3. This may be associated with the presence of higher proportions of DW in G1 as compared with G2 and G3. In addition to the endothermic peak at ~90°C, a secondary endothermic peak was observed in all the organogels [marked by an arrow in Figure 10(a)]. The secondary endothermic peak may be associated with the bound DW molecules. The secondary endothermic peaks of G1, G2, and G3 were at ~105°C, ~95°C, and 95°C, respectively. The presence of the secondary endothermic peak at higher temperature in G1 as compared with G2 and G3 may be attributed to the presence of higher W/OG ratio which resulted in the higher degree of intermolecular hydrogen bonding (as evident from FTIR and XRD studies).

Table VII. Textural Properties of the Organogels (Stress Relaxation Parameters)

Samples	F_0 (g)	F_{30} (g)	Work on relaxation (g.s)	% SR[a]
G1	39.543	16.985	589.866	42.953
G2	24.681	9.952	340.352	40.323
G3	25.344	11.279	386.371	44.503

[a] $SR = \frac{F_0 - F_{30}}{F_0}$.

Table VIII. Textural Properties of the Organogels (Spreadability Parameters)

Samples	Cohesiveness (g s)	Spreadability (g^{-1} s^{-1}) × 10^{-4}
G1	1887.882	5.3
G2	488.022	20.5
G3	1530.773	6.53

The DSC profiles of the microemulsions have been provided in Figure 10(b). All the microemulsions have shown a broad endothermic peak at ~75°C. This endothermic peak may be associated with the evaporation of the water molecules from the emulsion. Apart from the endothermic peak of evaporation of DW, M2 has shown an exothermic peak at ~35°C. This exothermic peak may be due to the presence of higher proportions of DW within M2 which resulted in the higher intermolecular hydrogen bonding. Hence, during heating of the M2 sample, there was disruption of the intermolecular hydrogen bonding before the evaporation of the water molecules was started.

Texture Analysis

The strength of the organogels was measured using a 30 mm aluminium platen and the results have been shown in Figure 11(a) and tabulated in Table VI. The results suggested that the strength and rigidity of G1 was highest. This may be associated to the presence of spherulites of gelator fibers, which might have lead to the improved mechanical properties of the organogel. The XRD studies also suggested that the crystallinity of the G1 was highest. The mechanical property of G3 was intermediate followed by G2. This can be explained due to reduction in the number of fluid-filled fibers in G3 followed by G2 (as observed under BFM) and reduction in crystallinity in G3 followed by G2 (as observed from XRD studies). The results indicated that the presence of fluid-filled fibers increased the crystallinity of the organogels, which in turn, was responsible for the variations in the mechanical properties of the organogels. Lower negative peak values of gel strength profile are related to stickiness whereas the area under the negative peaks provides information about the adhesiveness of the organogels. The stickiness and the adhesiveness of the organogels also followed similar pattern as that of gel strength, i.e., the stickiness and adhesiveness was in the order of G1>>G3>G2.

The stress relaxation (SR) profiles of the organogels have been shown in Figure 11(b) and the properties have been tabulated in Table VII. SR properties of the organogels were studied by applying stress on the organogels. In the study, the probe was allowed to move a distance of 10 mm after a trigger force of 5 g. The force at the said distance was regarded as F_0. The probe was allowed to stay at the same position for 30 s. The change in the force after 30 s hold time was regarded as F_{30}. The %age decrease in the force was regarded as % SR and is a measure of molecular rearrangement which occurs in the samples so as to

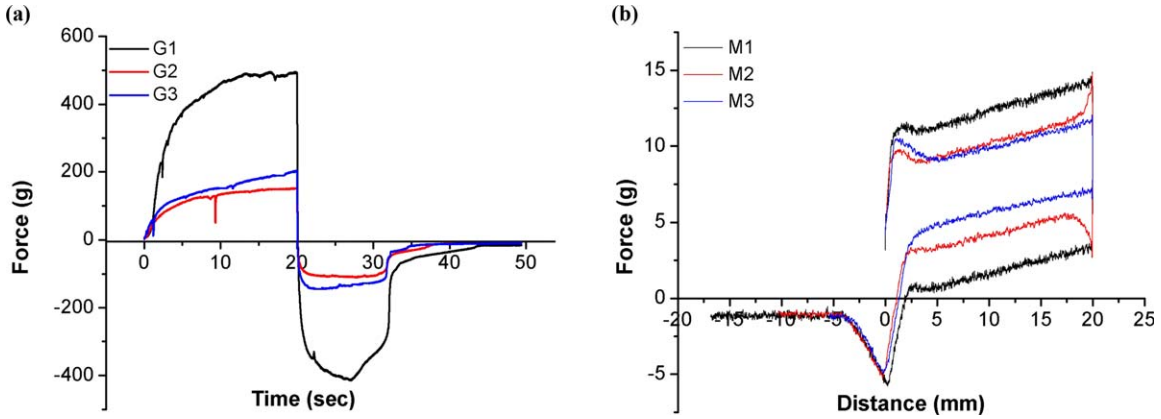

Figure 12. Textural properties determined by BE study. (a) Organogels and (b) microemulsions. [Color figure can be viewed in the online issue, which is available at wileyonlinelibrary.com.]

Table IX. Textural Properties of the Organogels (BE Parameters)

Sample	Firmness (g)	Cohesiveness (g)	Index of viscosity (g s)
G1	495.079	−414.932	8036.0
G2	152.7301	−110.534	2412.2
G3	203.5516	−128.314	2881.0

Table X. Textural Properties of the Microemulsions (BE Parameters)

Samples	Coefficient of viscosity (mPa s)
M1	0.040843
M2	0.03116
M3	0.019541

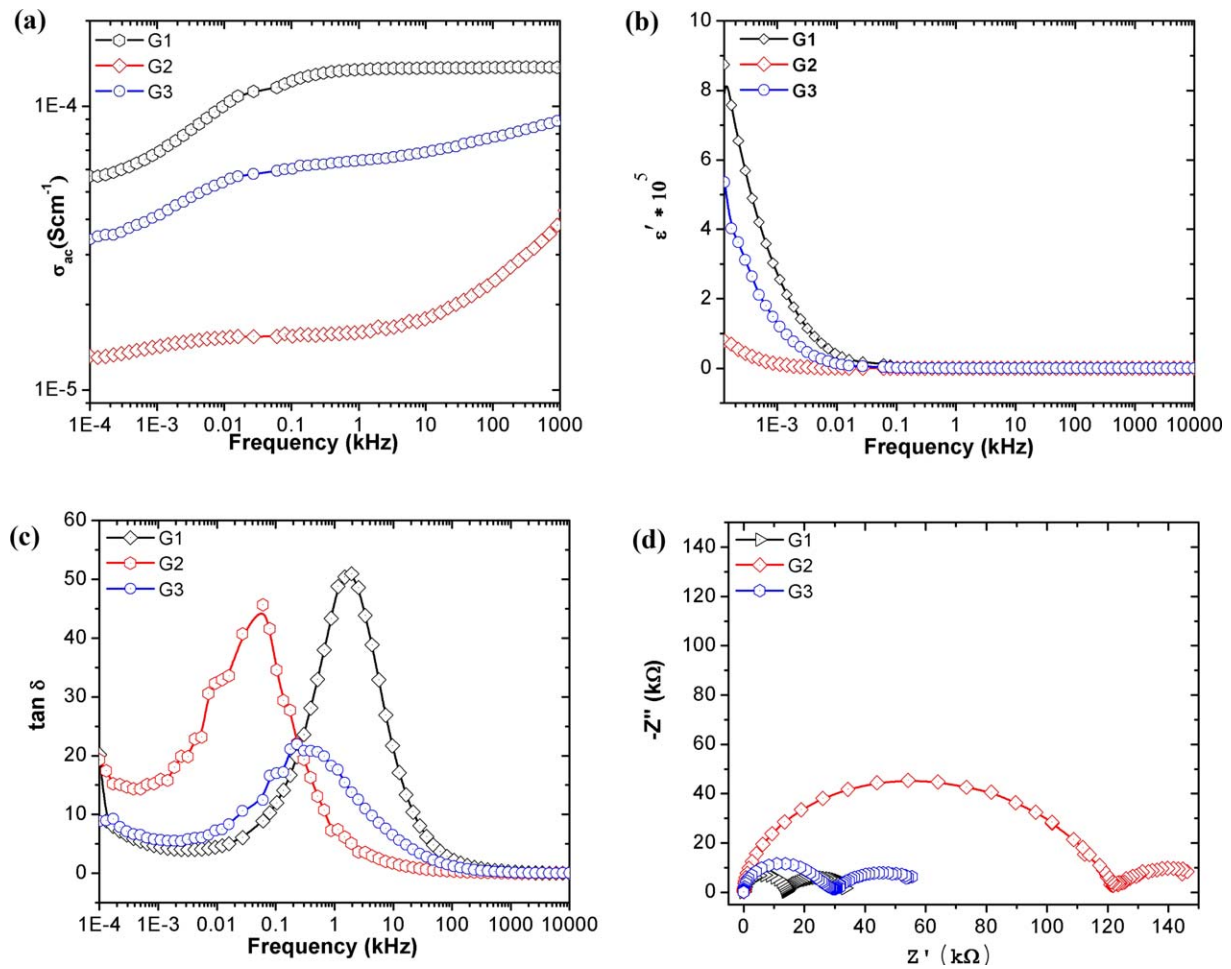

Figure 13. Electrical properties of the organogels. [Color figure can be viewed in the online issue, which is available at wileyonlinelibrary.com.]

Table XI. DC Conductivity (60) of the Organogels

Formulations	dc conductivity (σ_0) ($\times 10^{-5}$) (S cm^{-1})
G1	13.55
G2	1.54
G3	6.20

absorb the applied stress. The %SR was in the order of G3>G1>G2. This suggested that the molecular rearrangement of the fluid-filled network structure was higher when either fibers or globular structures were predominant. The presence of mixed structures reduced the chances of molecular rearrangement. The work done during the relaxation process was calculated from the area under the curve between F_0 and F_{30}. The work done during the relaxation of the organogels was in the order of G1>>G3>G2. The results supported the rigidity of the organogels calculated from the gel strength study.

The spreadability profiles of the organogels have been shown in Figure 11(c) and the properties have been tabulated in Table VIII. As a matter of fact, higher the rigidity of the gels, lower is the spreadability. Rigidity of the organogels is related to cohesiveness of the organogels.[41] The area under the positive peak is regarded as cohesiveness. The cohesiveness of the organogels was found to be in the order of G1>G3>G2. This is in accordance with the results obtained from the gel strength and the SR studies. Spreadability of the organogels is inversely related to cohesiveness [42]. Hence the spreadability was in the order G2>G3>G1.

The organogels and the microemulsions were also characterized by BE studies at RT (Figure 12). The BE studies of the organogels supported that the firmness and rigidity of the organogels were in the order of G1>>G3>G2 (positive peak) (Table IX). The area under the negative peak provides information about the index of viscosity of the organogels. In general, higher the firmness and rigidity of the gels, higher is the viscosity. The results suggested that the index of viscosity of G1 was highest followed by G3 and G2, i.e., the viscosity of the organogels was in the order of G1>> G3 > G2.

The calculation of viscosity of liquid samples is different. Fluids show a linear force vs. distance profile when the probe was

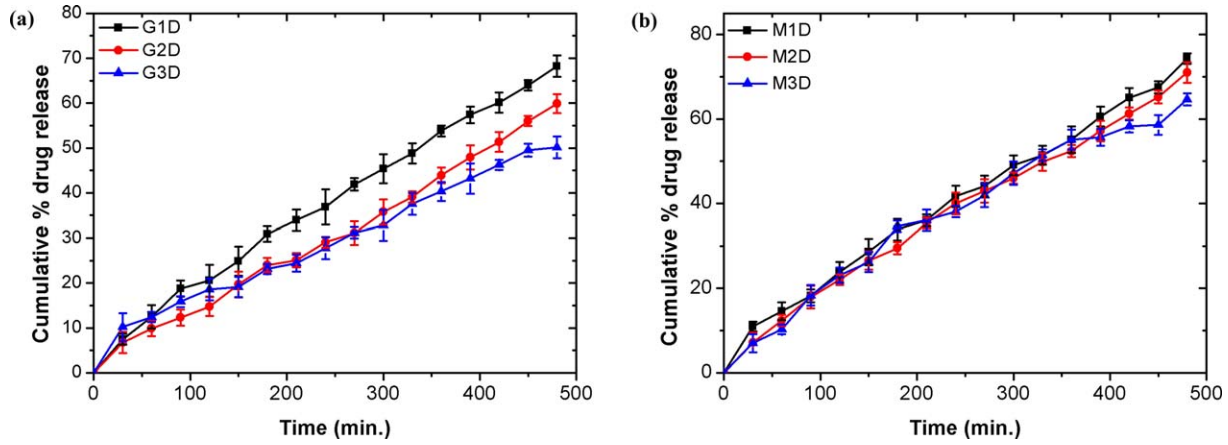

Figure 14. Drug release profiles. (a) Organogels and (b) microemulsions. [Color figure can be viewed in the online issue, which is available at wileyonlinelibrary.com.]

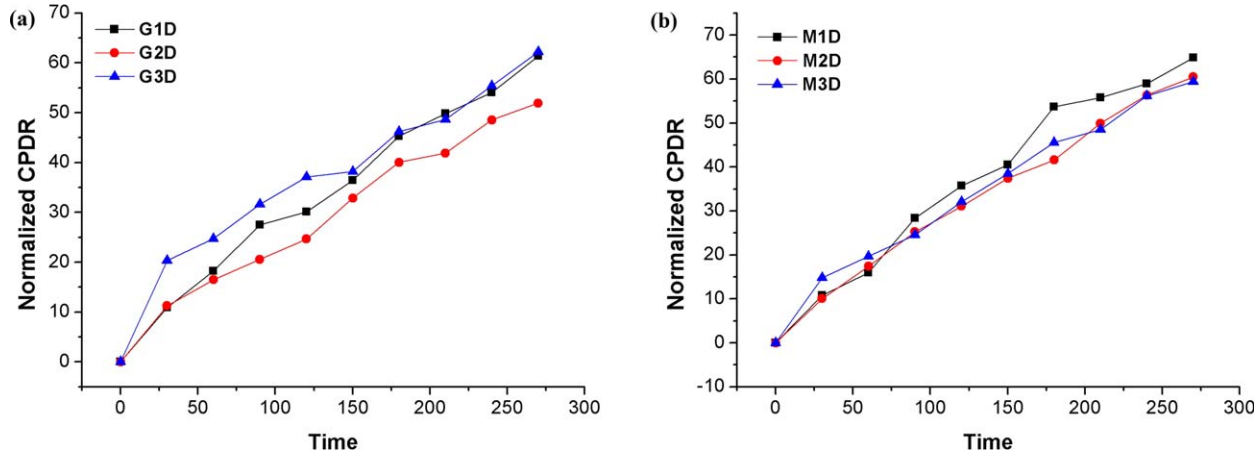

Figure 15. Zero-order kinetics plot. (a) Organogels and (b) microemulsions. [Color figure can be viewed in the online issue, which is available at wileyonlinelibrary.com.]

Table XII. Drug Release Kinetics Model Fitting

	r^2 for model fitting				
S no.	Zero order model	First order model	Higuchi model	KP model	Best fit
G1D	0.995	0.987	0.956	0.998	Zero order
G2D	0.995	0.971	0.945	0.995	Zero order
G3D	0.987	0.985	0.981	0.981	Zero order
M1D	0.992	0.987	0.947	0.996	Zero order
M2D	0.993	0.983	0.951	0.997	Zero order
M3D	0.973	0.992	0.965	0.992	First order

either being inserted or retracted out of the liquid sample. The slope of the force vs. distance profile, when the probe was retracting back was used for the calculation of the apparent viscosity as per the eq. (3). DW was used as a reference sample. The calculated coefficient of viscosity of microemulsions has been provided in Table X. The coefficient of viscosities of microemulsions was in the order of M1>M2>M3.

Electrical Properties of the Organgels

The frequency dependent variations of AC conductivity ($б_{ac}$) of the selected organogels have been shown in Figure 13(a). The results showed an increase in the conductivity as the frequency of the injecting current was increased. The low frequency dispersion may be associated with the electrode polarization at the sample-electrode interface.[43] The conductivity profiles suggested a capacitive dominant nature of the organogels. The DC conductivity of the organogels was determined and has been shown in Table XI. Both AC and DC conductivities of the organogels was in the order of G1 > G3 > G2. The results were in accordance with the R_b of the organogels.[44] The frequency dependent dielectric constant (ε') of the organogels has been plotted in Figure 13(b).[45] The ε' profile of the organogels showed a higher ε' at low frequency. There was a monotonically decrease in the ε' as the frequency was increased. The results confirmed the organogels had a capacitive dominant nature, as was observed from the AC conductivity profile.

The dielectric loss profile (tan δ) as a function of frequency has been shown in Figure 13(c). G2, G3 and G1 showed the maximum loss in the frequency range 10–100 Hz, 10^2–10^3 Hz, and 10^3–10^4 Hz, respectively.

The Nyquist plots (Z'' vs. Z') of G1, G2 and G3 have been shown in Figure 13(d). The organogels have shown formation of two semicircles. The intersection of the first semicircle with the x-axis provides information about the bulk resistance (R_b), a measure of the bulk properties of the organogels.[43,46] The second semicircle may be attributed to the grain boundary resistance.[47] The R_b of the organogels was in the order of G2 > G3 > G1. The results suggested that either with an increase in the OG proportion or a decrease in the water proportion there was an increase in the R_b.

In Vitro Drug Delivery Studies

The *in vitro* drug delivery studies were carried out using modified Franz's diffusion cell. The cumulative percentage drug release (CPDR) from the organogels and microemulsions has been shown in Figure 14. Organogels have shown 50–68% of CPDR, whereas microemulsions have shown 64–74% of CPDR. The lower CPDR from organogels may be due to the semisolid

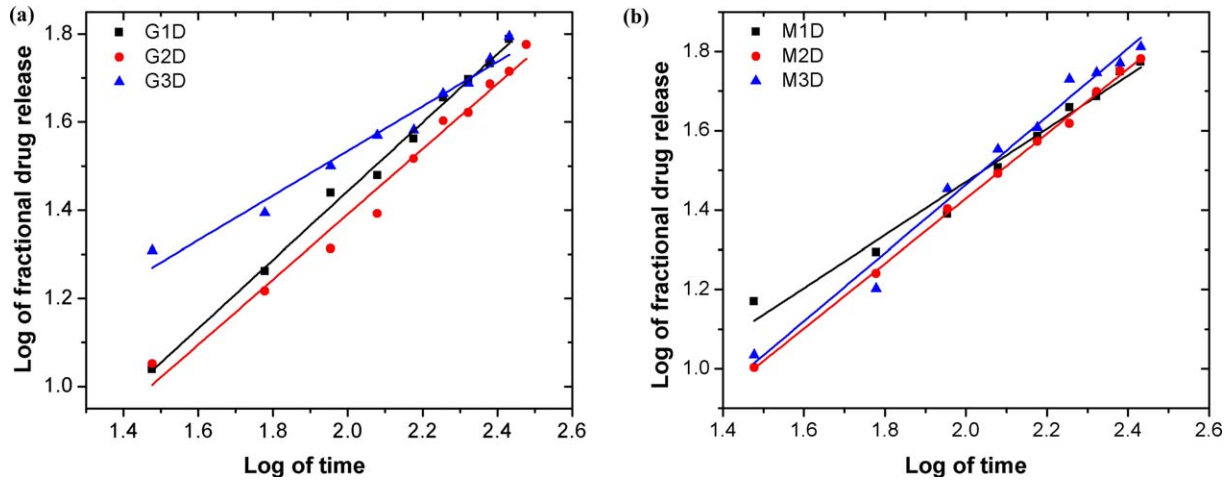

Figure 16. KP kinetics plot. (a) Organogels and (b) microemulsions. [Color figure can be viewed in the online issue, which is available at wileyonlinelibrary.com.]

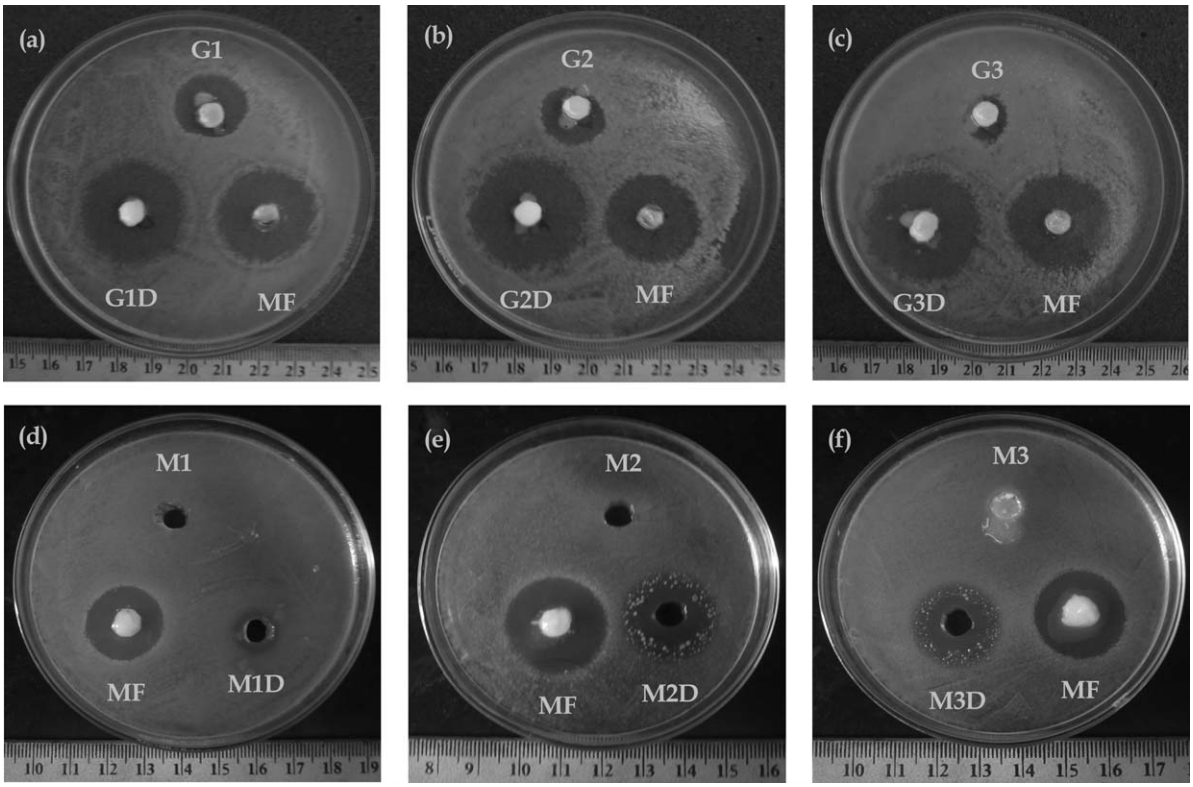

Figure 17. Antimicrobial activity of the drug loaded organogels (a-c) and microemulsions (d-f) against *B. subtilis*.

nature of the organogels. The gelator network of organogels might have restricted the free diffusion of the drugs. This feature facilitates the controlled delivery of drugs from the organogels. As microemulsions are devoid of gelator network structure, the release of the drug was higher in microemulsions. The higher drug release from microemulsions may also be due to the high surface-to-size ratio of the drug containing dispersed phase which might have improved the partitioning of the drug molecules and hence the drug release.

The drug release mechanism from the organogels and microemulsions was predicted. The drug release mechanism from all the formulations, except M3D, was found to follow zero order kinetics indicating that the release of the drug from the developed formulations was concentration independent (Figure 15, Table XII). M3D followed first order release kinetics. The release of the drug from the delivery systems was through diffusion.[48,49]

Table XIII. Antimicrobial Efficiency of the Drug-Loaded Organogels and Microemulsions

Sample	Zone of inhibition (cm)
G1D	3.0 ± 0.1
G2D	3.3± 0.2
G3D	3.2 ± 0.1
M1D	2.2 ± 0.2
M2D	2.1 ± 0.3
M3D	2.2 ± 0.2

Krossmeyer-Peppas (KP) model was used to understand the diffusion properties of the drugs by determining the Fickian value (n).[49] The "n" value for the organogels and the microemulsions was found to be in the range of 0.45–0.85.[48] This suggested that the drug release from the organogels and the microemulsions followed non-Fickian diffusion (Figure 16).

Antimicrobial Studies

The antimicrobial efficiency of the drug loaded organogels and microemulsions were tested against *B. subtilis* (Figure 17, Table XIII). The blank organogels and microemulsions have shown microbial activity. This may be attributed to the antimicrobial activity of the PO.[50] The antimicrobial activity was enhanced when drug was added. The antimicrobial efficiency of the drug-loaded organogels was found to be higher than the marketed formulation (MF; Ciplox®). The zone of inhibition of organogels and microemulsions was almost same.

CONCLUSIONS

The study reports the successful development of PO-based organogels and microemulsions using span 80/tween 80 mixture (OG) and DW. The formation of organogels was due to the self-organization of the fluid-filled structures. Heterogeneous nucleation was predominat during the formation of organogels. The thermal, physical, and mechanical properties of the organogels were dependent on the composition of the organogels. The microemulsion showed variations in the sizes of the dispersed phase and was dependent on the composition of the microemulsions. The organogels were viscoelastic in nature while the

microemulsions showed viscous flow. Both types of the formulations were found to be hemocompatible. The drug-loaded formulations showed equivalent antimicrobial activity as that of Ciplox (marketed formulation). In gist, the developed formulations may be tried in controlled drug delivery.

ACKNOWLEDGMENTS

The financial support provided by Department of Biotechnology, New Delhi, India vide sanction order (BT/PR14282/PID/06/598/2010) is acknowledged.

REFERENCES

1. Kumarand, R.; Katare, O. P. *AAPS PharmSciTech*, **2005**, *6*, 298.
2. Da Pieve, S.; Calligaris, S.; Co, E.; Nicoliand, M. C.; Marangoni, A. G. *Food Biophys.*, **2010**, *5*, 211.
3. Kulyginand, O.; Silverstein, M. S. *Soft Matter*, **2007**, *3*, 1525.
4. Pal, K.; Banthiaand, A.; Majumdar, D. *Mater. Manufacturing Proc.* **2006**, *21*, 877.
5. Mishra, R.; Datt, M.; Paland, K.; Banthia, A. *J. Mater. Sci.: Mater. Med.* **2008**, *19*, 2275.
6. Pal, K.; Banthiaand, A. K.; Majumdar, D. K. *Biomed. Mater.* **2006**, *1*, 49.
7. Vintiloiuand, A.; Leroux, J. C. *J. Control. Release* **2008**, *125*, 179.
8. Behera, B.; Patil, V.; Sagiri, S.; Paland, K.; Ray, S. *J. Appl. Polym. Sci.* **2012**, *125*, 852.
9. Xuan, X. Y.; Chengand, Y. L.; Acosta, E. *Pharmaceutics* **2012**, *4*, 104.
10. Peltola, S.; Saarinen-Savolainen, P.; Kiesvaara, J.; Suhonenand, T.; Urtti, A. *Int. J. Pharma.* **2003**, *254*, 99.
11. Lee, P. J.; Langerand, R.; Shastri, V. P. *Pharmaceutical Res.*, **2003**, *20*, 264.
12. Vintiloiuand, A.; Leroux, J.-C. *J. Control. Release* **2008**, *125*, 179.
13. Suzuki, M.; Nakajima, Y.; Yumoto, M.; Kimura, M.; Shiraiand, H.; Hanabusa, K. *Langmuir* **2003**, *19*, 8622.
14. Ajayaghoshand, A.; Praveen, V. K. *Accounts Chem. Res.* **2007**, *40*, 644.
15. Shirakawa, M.; Fujitaand, N.; Shinkai, S. *J. Am. Chem. Soc.* **2003**, *125*, 9902.
16. Liu, Q.; Rauthand, A. M.; Wu, X. Y. *Int. J. Pharma.* **2007**, *339*, 148.
17. Murdan, S. *Expert Opinion Drug Deliv.* **2005**, *2*, 489.
18. Kohand, L. P.; Wilcove, D. S. *Conservation Lett.* **2008**, *1*, 60.
19. Owen, D. H.; Petersand, J. J.; Katz, D. F. *Contraception* **2000**, *62*, 321.
20. Sagiri, S. S.; Behera, B.; Sudheepand, T.; Pal, K. *Designed Monomers Polym.* **2012**, *15*, 253.
21. Sagiri, S. S.; Behera, B.; Paland, K.; Basak, P. *J. Appl. Polym. Sci.* **2012**, n/a-n/a.
22. Bhattacharya, C.; Pal, K.; Kumar, N.; Sagiriand, S.; Ray, S. *J. Pharmacy Bioallied Sci.* **2012**, *4*, 155.
23. Behera, B.; Patil, V.; Sagiri, S. S.; Paland, K.; Ray, S. S. *J. Appl. Polym. Sci.*, **2012**, *125*, 852.
24. Shah, D. K.; Sagiri, S. S.; Behera, B.; Paland, K.; Pramanik, K. *J. Appl. Polym. Sci.* **2013**, *129*, 793.
25. Hartley, C. W. S. *The Oil Palm*, **1967**.
26. Sadough, S. A.; Rahmaniand, M. R.; Pouyafar, V. *Trans. Nonferrous Metals Society of China* **2010**, *20*, s906.
27. Rout, S.; Hussian, A.; Lee, J.; Kimand, I.; Woo, S. *J. Alloys Compounds* **2009**, *477*, 706.
28. Nandini, D.; Chauhan, N.; Chandraand, A.; Pathak, K. *J. Young Pharmacists* **2009**, *1*, 285.
29. Flanagan, J.; Kortegaard, K.; Neil Pinder, D.; Radesand, T.; Singh, H. *Food Hydrocolloids* **2006**, *20*, 253.
30. Spernathand, A.; Aserin, A. *Adv. Colloid Interface Sci.* **2006**, *128–130*, 47.
31. Forgiarini, A.; Esquena, J.; Gonzálezand, C.; Solans, C. *Langmuir* **2001**, *17*, 2076.
32. Queste, S.; Salager, J. L.; Streyand, R.; Aubry, J. M. *J. Colloid Interface Sci.* **2007**, *312*, 98.
33. Lawrence, M. J.; Rees, G. D. *Adv. Drug Deliv. Rev.* **2012**, *64*, 175.
34. Singh, V.; Sharma, H.; Veerma, R.; Javedand, A.; Singh, M. *Asian J. Pharmaceutics* **2013**, *7*, 1.
35. Yan, X.; Zhuand, P.; Li, J. *Chem. Soc. Rev.* **2010**, *39*, 1877.
36. Angelico, R.; Ceglie, A.; Colafemmina, G.; Lopez, F.; Murgia, S.; Olssonand, U.; Palazzo, G. *Langmuir* **2004**, *21*, 140.
37. Waguespack, Y. Y.; Banerjee, S.; Ramannair, P.; Irvin, G. C.; Johnand, V. T.; McPherson, G. L. *Langmuir* **2000**, *16*, 3036.
38. Chen, W.; Yang, Y.; Leeand, C. H.; Shen, A. Q. *Langmuir* **2008**, *24*, 10432.
39. Hurle, D. T. Handbook of Crystal Growth; Elseiver: North Holland, **1993**.
40. Behera, B.; Sagiri, S. S.; Paland, K.; Srivastava, A. *J. Appl. Polym. Sci.* **2013**, *127*, 4910.
41. Scholl, B. J. *Psychological Sci.* **2003**, *14*, 498.
42. Bot, A. R.; den Adel; Roijers, E.; Regkos, C. *Food Biophys.* **2009**, *4*, 266.
43. Pradhan, D. K.; Choudhary, R.; Samantaray, B. *Express Polym. Lett.* **2008**, *2*, 630.
44. Pradhan, D. K.; Samantaray, B.; Choudhary, R. N. P.; Thakur, A. K. *Ionics* **2005**, *11*, 95.
45. Pradhan, A.; Zhang, K.; Hunter, D.; Dadson, J.; Loiutts, G.; Bhattacharya, P.; Katiyar, R.; Zhang, J.; Sellmyer, D. J.; Roy, U. *J. Appl. Phys.* **2005**, *97*, 093903.
46. Ramesh, S.; Wong, K. *Ionics* **2009**, *15*, 249.
47. Shukla, A.; Choudhary, R.; Thakur, A.; Pradhan, D. *Phys. B: Condensed Matter* **2010**, *405*, 99.
48. Sawant, P. D.; Luu, D.; Ye, R.; Buchta, R. *Int. J. Pharma.* **2010**, *396*, 45.
49. Philip, A.; Srivastava, M.; Pathak, K. *Drug Deliv.* **2009**, *16*, 405.
50. Ekwenye, U.; Ijeomah, C. *KMITL. Sci. J.* **2005**, *5*, 502.